Modeling and simulating methods for the desiccation cracking

Sayako Hirobe[1,a] and Kenji Oguni[1,b]

[1]Department of System Design Engineering, Keio University, Japan

[a]Corresponding author: s.hirobe@keio.jp

[b]oguni@sd.keio.ac.jp

ABSTRACT

The desiccation cracks can be observed on dry-out soil fields or other various materials under desiccation. These cracks have a net-like structure and tessellate the surface of the materials into polygonal cells. The averaged cell sizes change systematically depending on the size of the specimen. In spite of the varieties of the materials, these fundamental features of the cell topology are conserved. This implies the existence of the governing mechanism behind the desiccation crack phenomenon regardless of the material. In this paper, the desiccation crack phenomenon is modeled by the coupling of the desiccation, deformation, and fracture. We perform the simulations for the reproduction of the desiccation cracking based on this coupling model. In the simulation, the finite element analysis for the desiccation problem and the analysis of particle discretization scheme finite element method for the deformation and fracture problems are weakly coupled. The results of the simulation show the satisfactory agreements with the experimental observation in terms of the geometry of the crack pattern, the increase tendency of the averaged cell size depending on the size of the specimen, and the hierarchical sequence of the cell formation. These agreement indicate that the proposed model and method capture the fundamental features and mechanism of the desiccation cracking.

Keywords: Desiccation cracks, Pattern formation, Coupled problem, PDS-FEM.

Introduction

The desiccation cracks can be observed on dry-out soil fields or other various materials under desiccation. These cracks have a net-like structure and tessellate the surface of the materials into polygonal cells with almost constant size and the averaged cell sizes change systematically depending on the size of the specimen. These features of the desiccation cracks are searched on the various materials in previous researches [1]-[8]. In spite of the varieties of the materials, the fundamental features of the cell topology (i.e., the net-like structure of the cracks, the change in averaged cell size depending on the thickness of the specimen) are conserved. This conservation of the features implies the existence of the governing mechanism behind the desiccation crack phenomenon regardless of the choice of the materials. However, the experimental researches cannot explain this governing mechanism because the measurement of the local distribution of the physical quantities near the cracks such as the water content and the stress is still difficult. Thus, the numerical approaches are required for detailed quantitative discussion.

In previous researches, a number of models and analysis methods for the analysis of the desiccation crack phenomenon are proposed. Most of these models assume the homogeneous water distribution and ensuing uniform drying shrinkage [9]-[12]. While this assumption might be sufficient for the thin-layer specimen where the gradient of the water distribution can be neglected, it cannot be applied for the thick-layer specimen where the gradient of the water distribution remarkably appears. On the other hand, some models attempt to embed the inhomogeneous water distribution due to desiccation in the stress analysis [13][14]. However, these models and methods do not introduce the effect of the cracks in the desiccation and deformation problem. Thus, they can be regarded as the pseudo-coupling analysis. This pseudo-coupling analysis can reproduce the crack initiation or the final crack pattern in the limited case, the process of the crack pattern formation cannot be reproduced.

In this paper, the desiccation crack phenomenon is modeled as the coupling of the desiccation, deformation, and fracture. The desiccation problem and the deformation problem are described by the diffusion equation and the equation of force equilibrium respectively and the effect of fracture is embedded in each problem. We perform the simulations for the reproduction of the desiccation cracking based on this coupling model. In the simulation, the finite element analysis for the desiccation problem and the analysis of particle discretization scheme finite element method (PDS-FEM) [15][16] for the deformation and fracture problems are weakly coupled. The simulation results are compared with the results of drying experiments of calcium carbonate slurry to validate the proposed model and simulation method qualitatively. Throughout this paper, the summation convention is employed for the subscripts in the equation.

Drying Experiment of Calcium Carbonate Slurry

We performed the drying experiments of calcium carbonate slurry to observe the change in cell sizes depending on the thickness of the specimen and the pattern formation process of the desiccation cracking. The change in averaged volumetric water content was measured during desiccation for the determination of the parameters used in the numerical analysis. The saturated calcium carbonate slurry was prepared at the volumetric water content rate 72%. Then, the slurry was poured into the rectangular acrylic container; the size of the container was $100 \times 100 \times 50$ mm. The thickness of the specimen was set as 5 mm, 10 mm, 20 mm, and 30 mm. The slurry was dried at 20 °C temperature and at 50% relative humidity in the air until the entire of the specimen dried out completely.

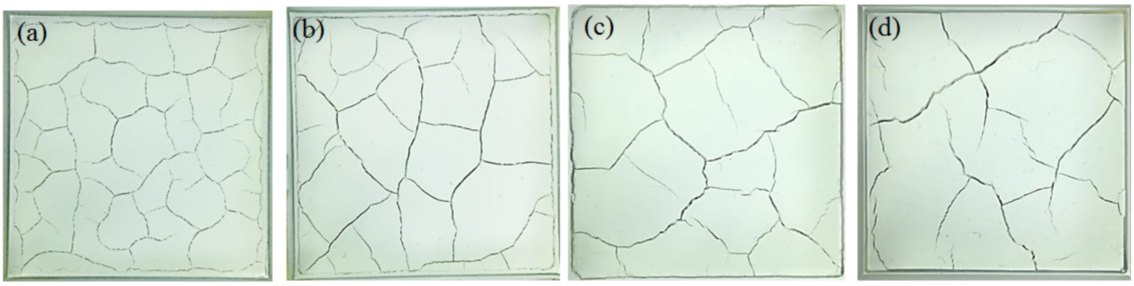

Figure 1. The final crack patterns formed on the top surface of the specimen after the desiccation with different thickness. (a) 5 mm, (b) 10 mm, (c) 20 mm, (d) 30 mm.

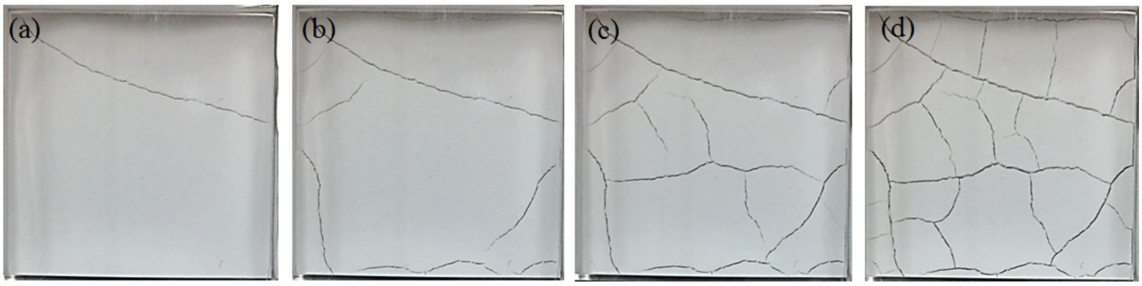

Figure 2. The cell formation process of the drying experiment in the case of 10 mm thickness. (a) the crack initiation, (b) the primary cracks growth, (c) the secondary cracks growth and the tessellation of the lager cells, (d) the final crack pattern.

During the desiccation, the excessive water layer on the top surface of the specimen disappeared at the volumetric water content 56.6% and the cracks initiated on the top surface of the specimen at the volumetric water content 22.4%. The pattern formation of the desiccation cracks terminated before the entire specimen dries out (at the volumetric water content 20.4%). Figure 1 shows the final patterns of cracks formed on the top surface of the specimen with different thickness. The size of the cells framed by the cracks is kept almost constant in each thickness and the averaged cell size increase with the increase of the thickness of the specimen. Figure 2 shows the pattern formation process of the cracks on the top surface of the specimen in the case of 10 mm thickness. On the initial stage of the desiccation cracking, some long and curved cracks initiate on the edge of the specimen and extend to the other edges traversing the specimen (Fig 2 (a) and (b)). These cracks (considered as the primary cracks) do not branch and form the largest structure of the cells. Then, relatively short cracks are formed and tessellate the lager cells (Fig 2 (c) and (d)). These cracks (considered as the secondary cracks) often branch and terminate when they meet the existing cracks. This hierarchical cell tessellation by the secondary cracks continues until the crack initiation terminates. During the desiccation, the volumetric water content reduced almost linearly.

Mathematical Model for Desiccation Cracking

Field Equations for Desiccation Cracking

The desiccation crack phenomenon can be regarded as the coupled problem of the desiccation, deformation, and fracture. For the formulation of this coupled model, we introduce the governing equations for the desiccation problem in fractured medium and the deformation problem in fractured medium.

The desiccation process of the mixture of the powder and the water can be expressed by the Richards' equation:

$$\frac{\partial\theta}{\partial t} = \nabla(D(\theta)\nabla\theta) + \frac{\partial K(\theta)}{\partial z} \tag{1}$$

where θ is a volumetric water content, t is time, $K(\theta)$ is an unsaturated hydraulic conductivity, and $D(\theta)$ is a moisture diffusion coefficient. When we assume the constant moisture diffusion coefficient and neglect the gravitational effect, the Richards' equation is simplified to the linear moisture diffusion equation in terms of the volumetric water content θ:

$$\frac{\partial\theta}{\partial t} = D\nabla^2\theta. \tag{2}$$

Here, the volumetric water content θ is a function of the position $\boldsymbol{x}$ and time t.

Consider a permeable and linearly elastic body Ω with external boundary $\partial\Omega$. When the initial volumetric water content in Ω is set as $\theta^0(\boldsymbol{x})$ and the water evaporates from the external boundary $\partial\Omega$, the desiccation process in Ω is expressed as the next initial boundary value problem:

$$\begin{cases} \dot{\theta} = D\nabla^2\theta & \boldsymbol{x} \in \Omega \quad (3a) \\ \theta(\boldsymbol{x}, 0) = \theta^0(\boldsymbol{x}) & \boldsymbol{x} \in \Omega \quad (3b) \\ D\dfrac{\partial\theta}{\partial\boldsymbol{n}} = -q^{\Omega}(\boldsymbol{x}, t) & \boldsymbol{x} \text{ on } \partial\Omega \quad (3c) \end{cases}$$

where $q^{\Omega}(\boldsymbol{x}, t)$ is a water flux due to evaporation from the external boundary $\partial\Omega$. In the desiccation problem, the crack surfaces Γ can be regarded as the newly created evaporation surfaces. Therefore the effect of cracks on the desiccation process is embedded as the Neumann boundary condition:

$$D\frac{\partial\theta}{\partial\boldsymbol{n}} = -q^{\Gamma}(\boldsymbol{x}, t) \qquad \boldsymbol{x} \text{ on } \Gamma \tag{4}$$

where $q^{\Gamma}(\boldsymbol{x}, t)$ is a water flux due to evaporation from the crack surfaces Γ.

On the other hand, the deformation process of an isotropic and elastic body Ω corresponding to the change in the volumetric water content θ given by the initial boundary value problem (3) is governed by the equation of force equilibrium:

$$\begin{cases} \sigma_{ij,j} = 0 & \boldsymbol{x} \in \Omega \quad (5a) \\ \sigma_{ij} = c_{ijkl}(\varepsilon_{kl} - \varepsilon^s_{kl}) & \boldsymbol{x} \in \Omega \quad (5b) \\ \varepsilon_{ij} = \dfrac{1}{2}(u_{i,j} + u_{j,i}) & \boldsymbol{x} \in \Omega \quad (5c) \end{cases}$$

where σ_{ij} is a stress, c_{ijkl} is a elastic modulus, ε_{ij} is a total strain, ε^s_{ij} is a shrinkage strain, and u_i is a displacement. In the case of the drying shrinkage, since the drying shrinkage strain ε^s_{ij} resulting from the volume reduction due to desiccation is inelastic, the drying shrinkage strain does not contribute to the generation of the stress. Therefore, the elastic strain $\varepsilon^e_{ij} = \varepsilon_{ij} - \varepsilon^s_{ij}$ becomes the source of the stress instead of the total strain ε_{ij} as shown in Eq. (5b). This approach can be also seen in Peron et al.[14]. Considering the isotropy of Ω, the shrinkage strain ε^s_{ij} is derived from the volumetric drying shrinkage strain ε^v corresponding to the reduction of the volumetric water content θ as follows:

$$\varepsilon^v(\boldsymbol{x}, t) = \frac{1}{\alpha}\frac{\rho_w}{\rho_d}\{\theta(\boldsymbol{x}, t) - \theta(\boldsymbol{x}, 0)\} \tag{6}$$

$$\varepsilon^s_{ij} = \frac{1}{3}\varepsilon^v\delta_{ij} \tag{7}$$

where ρ_w is the mass density of the water, ρ_d is the dry bulk density of the powder, α is the moisture shrinkage coefficient of the powder and δ_{ij} is the Kronecker's delta.

When the displacement boundary condition $\bar{u}_i(\boldsymbol{x})$ is prescribed on the external boundary $\partial\Omega$, the deformation process of Ω is given by the next boundary value problem:

$$\begin{cases} \sigma_{ij,j} = 0 & \boldsymbol{x} \in \Omega & \text{(8a)} \\ \sigma_{ij} = c_{ijkl}(\varepsilon_{kl} - \varepsilon^s_{kl}) & \boldsymbol{x} \in \Omega & \text{(8b)} \\ \varepsilon_{ij} = \dfrac{1}{2}(u_{i,j} + u_{j,i}) & \boldsymbol{x} \in \Omega & \text{(8c)} \\ u_i = \bar{u}_i & \boldsymbol{x} \text{ on } \partial\Omega^u. & \text{(8d)} \end{cases}$$

In the deformation problem, the crack surfaces Γ can be regarded as the traction-free surfaces and the effect of crack surfaces Γ is embedded as

$$\sigma_{ij}n_j = 0 \quad \boldsymbol{x} \text{ on } \Gamma \tag{9}$$

where n_i is a unit normal vector of the crack surfaces Γ.

Thus, the problems of desiccation and deformation in fractured medium are coupled by Eq. (6) (the relationship between volumetric water content and volumetric shrinkage strain) and embedding the effect of common crack surfaces in each problem.

Discretized Form of the Field Equations of Desiccation Cracking

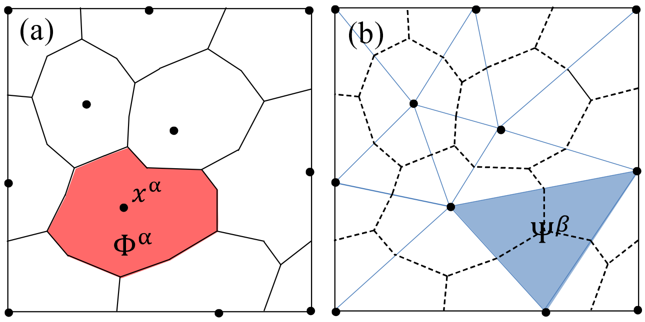

Figure 3. The discretization of the analysis domain Ω in two-dimension. (a) Volonoi tessellations Φ^α, (b) The Delaunay tessellations Ψ^β.

In this research, the analysis of the deformation and fracture are performed by using PDS-FEM. PDS-FEM applies the particle discretization for the variables using a discontinuous and non-overlapping characteristic functions defined on the Voronoi blocks $\{\Phi^\alpha\}$ and the Delaunay tetrahedrons $\{\Psi^\beta\}$; this conjugate pair of geometries are uniquely defined for the set of nodes $\{\boldsymbol{x}^\alpha\}$ as shown in Fig. 3. In two-dimension, the Delaunay block becomes a triangle. The characteristic functions are defined as

$$\phi^\alpha(\boldsymbol{x}) = \begin{cases} 1 & (\boldsymbol{x} \in \Phi^\alpha) \\ 0 & (\boldsymbol{x} \notin \Phi^\alpha) \end{cases} \tag{10}$$

$$\psi^\beta(\boldsymbol{x}) = \begin{cases} 1 & (\boldsymbol{x} \in \Psi^\beta) \\ 0 & (\boldsymbol{x} \notin \Psi^\beta). \end{cases} \tag{11}$$

Then, the displacement u_i and the strain ε_{ij} are discretized as

$$u_i(\boldsymbol{x}) = \sum_{\alpha=1}^{N} u_i^\alpha \phi^\alpha(\boldsymbol{x}) \tag{12}$$

$$\varepsilon_{ij}(\boldsymbol{x}) = \sum_{\beta=1}^{M} \varepsilon_{ij}^\beta \psi^\beta(\boldsymbol{x}) \tag{13}$$

where N is a number of Voronoi blocks and M is a number of Delaunay tetrahedrons. Thus, the displacement is discretized by the Voronoi blocks $\{\Phi^\alpha\}$ and the variables related to the spatial gradient of the displacement (i.e., strain and stress) are averaged over the Delaunay tetrahedrons $\{\Psi^\beta\}$.

The boundary value problem (8) for the deformation problem is equivalent to the next variational problem:

$$\mathrm{I}(u_i(\boldsymbol{x})) = \int_{\Omega} \frac{1}{2}\left(\varepsilon_{ij} - \varepsilon^{s}_{ij}\right) c_{ijkl} \left(\varepsilon_{kl} - \varepsilon^{s}_{kl}\right) dV$$
$$\text{Minimize } \mathrm{I}(u_i(\boldsymbol{x})) \text{ s.t. } u_i(\boldsymbol{x}) = \bar{u}_i(\boldsymbol{x}) \text{ on } \partial\Omega \tag{14}$$

Applying the particle discretization scheme to this functional I, the discretized functional Î becomes

$$\hat{\mathrm{I}} = \sum_{\beta=1}^{M} \frac{1}{2}\left(\varepsilon^{\beta}_{ij} - \varepsilon^{s\beta}_{ij}\right) c^{\beta}_{ijkl} \left(\varepsilon^{\beta}_{kl} - \varepsilon^{s\beta}_{kl}\right) \Psi^{\beta} \tag{15}$$

where Ψ^{β} is the volume of the β-th Delaunay block.

In PDS-FEM, the strain-displacement relation is expressed as

$$\varepsilon^{\beta}_{ij} = \sum_{\alpha=1}^{N} \frac{1}{2}(B^{\beta\alpha}_{j} u^{\alpha}_{i} + B^{\beta\alpha}_{i} u^{\alpha}_{j}) \tag{16}$$

where

$$\begin{aligned} B^{\beta\alpha}_{i} &= \frac{1}{\Psi^{\beta}} \int_{\Psi^{\beta}} \phi^{\alpha}_{,i}(\boldsymbol{x}) \psi^{\beta}(\boldsymbol{x}) dV \\ &= \frac{1}{\Psi^{\beta}} \int_{\partial\Psi^{\beta}} n^{\alpha}_{i}(\boldsymbol{x}) dS \\ &= \frac{1}{\Psi^{\beta}} \int_{\partial\Phi^{\alpha}\cap\Psi^{\beta}} n^{\alpha}_{i}(\boldsymbol{x}) dS. \end{aligned} \tag{17}$$

Note that $B^{\beta\alpha}_{i}$ is identical to the B matrix for the strain field in the ordinary FEM with the linear tetrahedral elements. Applying this strain-displacement relation to the discretized functional Î in Eq. (15), the discretized functional Î can be expressed in terms of the nodal displacement u^{α}_{i}. Then, the stationary condition for Î results in the equation of force equilibrium

$$\sum_{\gamma=1}^{N} K^{\alpha\gamma}_{ik} u^{\gamma}_{k} = f^{\alpha}_{i}, \tag{18}$$

where stiffness matrix $K^{\alpha\gamma}_{ij}$ and external force vector f^{α}_{i} is

$$K^{\alpha\gamma}_{ik} = \sum_{\beta=1}^{M} B^{\beta\alpha}_{j} c^{\beta}_{ijkl} B^{\beta\gamma}_{l} \Psi^{\beta} \tag{19}$$

$$f^{\alpha}_{k} = \sum_{\beta=1}^{M} \varepsilon^{s\beta}_{ij} \left(c^{\beta}_{ijkl} B^{\beta\alpha}_{l}\right) \Psi^{\beta}. \tag{20}$$

In PDS-FEM, fracture is expressed as the loss of the interaction between Voronoi blocks and the fracture surfaces are defined on the boundary of Voronoi blocks (i.e., in the Delaunay tetrahedron). The loss of the interaction between Voronoi blocks is expressed as the removal of the contribution of the nodal displacement to the strain averaged over the fractured Delaunay tetrahedron. Thus, $B^{\beta\alpha}_{i}$ related to the Delaunay tetrahedron and Voronoi blocks composing the fracture surface becomes zero. The effect of this removal of $B^{\beta\alpha}_{i}$ is finally embedded in the stiffness matrix $K^{\alpha\gamma}_{ij}$. Thus, the Neumann boundary condition (9) on crack surfaces Γ (i.e., traction-free surface) is introduced as the change in the stiffness matrix $K^{\alpha\gamma}_{ij}$ of the equation of force equilibrium (18) in discretized form of the deformation problem.

The analysis of desiccation process is performed by using the ordinary FEM with linear tetrahedral elements corresponding to the Delaunay tetrahedrons used in analysis of deformation and fracture by PDS-FEM. The initial boundary value problem (3) is spatially discretized by using the shape function for the linear tetrahedral elements. Therefore, the Eq. (6) expressing the relation between the volumetric water content and the volumetric drying shrinkage strain is discretized as

$$\varepsilon^{v\beta}(\boldsymbol{x}, t) = \frac{1}{\alpha} \frac{\rho_w}{\rho_d} \{\bar{\theta}^{\beta}(t) - \bar{\theta}^{\beta}(0)\} \tag{21}$$

where $\bar{\theta}^{\beta}$ (function of time t) is an average of the nodal volumetric water content consisting the β-th Delaunay tetrahedron.

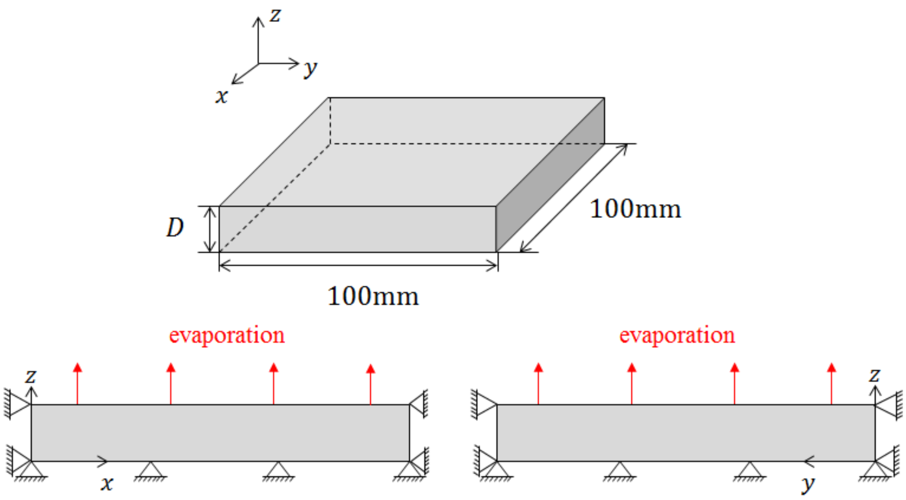

Figure 4. The geometry and the boundary conditions for the numerical analysis of the desiccation cracking.

For the introduction of the Neumann boundary condition (4) to the discretized form of the initial boundary value problem (3), the expression of the crack surfaces on PDS-FEM is applied to the FEM analysis of the desiccation process. Thus, the crack surfaces Γ is defined on the boundary of Voronoi blocks. The Neumann boundary condition (4) can be interpreted as i) elimination of the water flux normal to the crack surfaces Γ and ii) the prescribed water flux q^Γ due to evaporation on the crack surfaces Γ. The elimination of the water flux normal to Γ can be introduced as the anisotropic moisture diffusion coefficient. The water flux vector $\boldsymbol{J}$ in the orthonormal coordinate system $\{\boldsymbol{e}_i\}$ is expressed by Darcy's law:

$$\boldsymbol{J} = -D\nabla\theta. \tag{22}$$

We set the orthonormal coordinate system $\{\boldsymbol{e}'_i\}$ with $\boldsymbol{e}'_3$ in the normal direction of the crack surface Γ. The components of the projection of $\boldsymbol{J}$ on Γ (denoted as $\boldsymbol{J}^c$) in the $\{\boldsymbol{e}_i\}$ coordinate system is

$$J^c_i = T_{ji}P_{jk}T_{kl}J_l \tag{23}$$

where coordinate transform matrix T_{ij} and the projection matrix P_{ij} are

$$T_{ij} = \boldsymbol{e}'_i \cdot \boldsymbol{e}_j \tag{24}$$

$$P_{ij} = \begin{cases} 1 & \text{if } i = j = 1, 2 \\ 0 & \text{otherwize.} \end{cases} \tag{25}$$

Thus, the elimination of the water flux normal to Γ (i.e., the replacement of $\boldsymbol{J}$ with $\boldsymbol{J}^c$) corresponds to the introduction of the anisotropic moisture diffusion coefficient ($DT_{ji}P_{jk}T_{kl}$) to the fractured tetrahedral elements.

Since nodes are not placed on the crack surfaces expressed in the analysis of PDS-FEM, the water flux q^Γ is prescribed on the nodes placed on the boundary of fractured tetrahedral elements and unfractured tetrahedral elements. This prescription of the water flux corresponds to the assumption of the blunt crack.

Numerical Analysis of Desiccation Cracking

We perform the simulations for the reproduction of the crack patterns and the cell formation process observed in the drying experiments of calcium carbonate slurry. The distribution of the volumetric water content is obtained by the FEM analysis for the initial boundary value problem (3) with a constant time step $\Delta t = 0.1$ hour. Then, the seamless analysis for the deformation and the fracture by PDS-FEM is performed at each time step. Since the time scale for the desiccation and the fracture have a strong contrast, we performed the weak coupling analysis for these problems (i.e., weak coupling of the FEM analysis and the analysis of PDS-FEM). To capture the effect of the fracture surfaces promptly, the time step is reduced to $\Delta t = 0.01$ hour when the maximum traction among all elements reached to the 97% of the tensile strength t_c.

The model sizes and the boundary conditions is set to fit the drying experiments of calcium carbonate slurry; see Fig. 4 The thickness is set as 5 mm, 10 mm, 20 mm, and 30 mm. The nodal displacement of the sides and the bottom surfaces of

Table 1. Mesh sizes for the numerical analysis of the desiccation cracking

model size [mm]	number of elements	number of nodes
$100 \times 100 \times 5$	253,930	50,355
$100 \times 100 \times 10$	278,337	51,726
$100 \times 100 \times 20$	309,509	55,304
$100 \times 100 \times 30$	347,551	61,146

Table 2. The parameters for the numerical analysis of the desiccation cracking

parameters	
Soil dry density ρ_g	$800\,\mathrm{kg/m^3}$
Initial volumetric water content θ^0	0.560
Volumetric water content at the end of the simulation θ^f	0.204
Evaporation speed on the top surface q^Ω	$8.8 \times 10^{-5}\,\mathrm{m/hour}$
Evaporation speed of the crack surfaces q^Γ	$4.4 \times 10^{-5}\,\mathrm{m/hour}$
Moisture shrinkage coefficient α	0.69
Moisture diffusion coefficient D	$3.6 \times 10^{-6}\,\mathrm{m^2/hour}$
Poisson's ratio ν	0.3
Young's modulus E	5.0 MPa
Tensile strength t_c	1.6 MPa

the analysis model are constrained in all directions to express the adhesion between the slurry and the container wall on the drying experiments. The water evaporates from the top surface of the analysis model and crack surfaces. We prepare the finite element models with unstructured mesh for each model; the mesh sizes are shown in Table 1.

The measurable parameters are determined from the drying experiments of calcium carbonate slurry; see Table 2. The initial volumetric water content is set as the volumetric water content at which the excessive water layer disappeared in the drying experiments. The analysis is stopped when the volumetric water content reach to the 20.4% at which the crack pattern formation terminated in the drying experiments. The other parameters which are not measured in the drying experiments of calcium carbonate slurry (Young's modulus, tensile strength, and the moisture diffusion coefficient) are determined from the drying experiments of clayey silt in previous researches[6]. The evaporation speed on the crack surfaces q^Γ can be considered as slower than that on the top surface q^Ω because the opening width of the cracks is narrow. Therefore, the evaporation speed on the crack surfaces q^Γ is set as 50% of q^Ω.

Figure 5 shows the final crack patterns formed on the top surface of the analysis models with different thickness. The cracks have net-like structure and form polygonal cells. The cell sizes are kept almost constant on each thickness and the averaged cell size increases with the increase of the thickness. These geometric features of the crack pattern (i.e., net-like structure and polygonal cells) and the increasing tendency of the cell sizes depending on the thickness of the analysis model can be also observed in the drying experiment of calcium carbonate slurry.

The cell formation process on the top surface of the analysis model in the case of 10 mm thickness is shown in Fig. 6. In the early stage of the desiccation process, some long cracks initiate on the edge of the analysis model and extend traversing the top surface (Fig.4 (a) and (b)). These cracks can be considered as primary cracks observed on the drying experiment of calcium carbonate slurry. Then, relatively short cracks propagate to tessellate the lager cells (Fig.4 (c) and (d)). These cracks often branch and propagate until they meet other cracks; the emergence of the secondary cracks. The features of the shape of the cracks and the hierarchical sequence of the cell formation coincide with the drying experiment of calcium carbonate slurry.

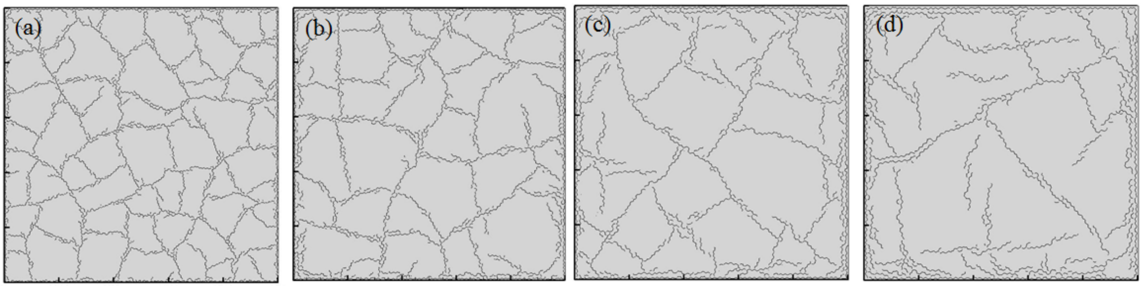

Figure 5. The final crack pattern formed on the top surface for each analysis model. (a) 5 mm, (b) 10 mm, (c) 20 mm, (d) 30 mm.

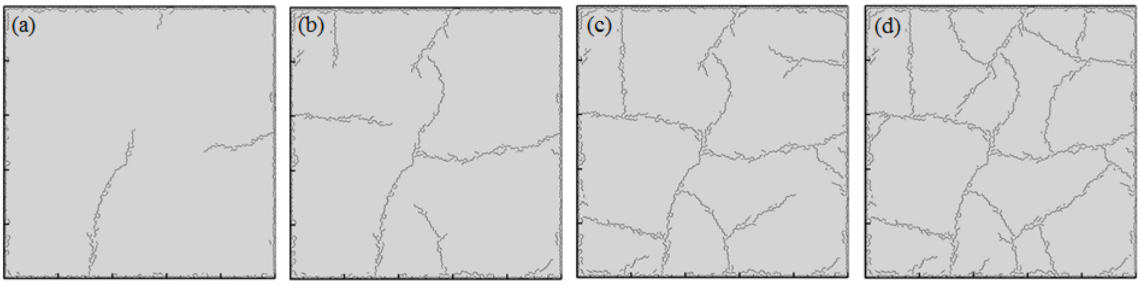

Figure 6. The cell formation process of the numerical analysis in the case of 10 mm thickness. (a) the crack initiation, (b) the primary cracks growth, (c) the secondary cracks growth and the tessellation of the lager cells, (d) the final crack pattern.

Conclusions

In this paper, the problem of the desiccation cracking is modeled by the coupling of desiccation, deformation, and fracture. In the proposed model, the diffusion equation with the anisotropic diffusion coefficient and the equation of the force equilibrium with the stiffness matrix reflecting the loss of the interaction due to fracture are coupled. This coupling analysis is performed by introducing the relation between volumetric drying shrinkage strain and embedding the effect of the common crack surfaces in desiccation and deformation problem.

The simulations with the FEM analysis and the analysis of PDS-FEM are performed to reproduce the crack patterns and the cell formation process observed in the drying test of calcium carbonate slurry. The simulation results show the satisfactory agreements with the experimental observation in terms of the geometry of the crack pattern, the increasing tendency of the averaged cell size depending on the thickness of the specimen, and the hierarchical sequence of the cell formation. These agreement indicate that the proposed model and method capture the fundamental features and mechanism of the desiccation cracking. For more quantitative discussion, we need the parametric study on the parameters which can not be measured in experiments.

References

[1] Corte, A. and Higashi, A. (1960). Experimental research on desiccation cracks in soil. Technical report, U.S. Army Snow Ice and Permafrost Research Establishment, Illinois, USA.

[2] Groisman, A. and Kaplan, E. (2006). An experimental study of cracking induced by desiccation. *Europhysics. Letters*, 25(6):415–420.

[3] Kindle, E. M. (1917). Some factors affecting the development of mud-cracks. *Journal of Geology*, 25:135–144.

[4] Kodikara, J. K., Barbour, S. L., and Fredlund, D. G. (2000). Desiccation cracking of soil layers. In *Unsaturated soils for Asia. Proceedings of the Asian Conference on Unsaturated Soils, UNSAT-ASIA 2000, Singapore, 18-19 May, 2000*, pages 693–698.

[5] Miller, C., Hong, M., and Nazli, Y. (1998). Experimental analysis of desiccation crack propagation in clay liners. *Journal of the American Water Resources Association*, 34(3):677–686.

[6] Peron, H., Hueckel, T., Laloui, L., and Hu, L. B. (2009). Fundamentals of desiccation cracking of fine-grained soils: experimental characterisation and mechanisms identification. *Canadian Geotechnical Journal*, 46(10):1177–1201.

[7] Rodríguez, R., Sánchez, M., Ledesman, A., and Lloret, A. (2007). Experimental and numerical analysis of desiccation of mining waste. *Canadian Geotechnical Journal*, 44(6):644–658.

[8] Vogel, H. J., Hoffmann, H., and Roth, K. (2005b). Studies of crack dynamics in clay soil I. experimental methods, result, and morphological quantification. *Geoderma*, 125:203–211.

[9] Sánchez, M., Manzoli, O. L., and Guimarães, L. J. N. (2014). Modeling 3-D desiccation soil crack networks using a mesh fragmentation technique. *Computers and Geotechnics*, 62:27–39.

[10] Sima, J., Jiang, M., and Zhou, C. (2014). Numerical simulation of desiccation cracking in a thin clay layer using 3D discrate element modeling. *Computers and Geptechnics*, 56:168–180.

[11] Trabelsi, H., Jamei, M., Zenzri, H., and Olivella, S. (2012). Crack patterns in clayey soils: Experiments and modeling. *International journal for numerical and analytical and methods in geomechanics*, 36:1410–1433.

[12] Vogel, H. J., Hoffmann, H., Leopold, A., and Roth, K. (2005a). Studies of crack dynamics in clay soil II. a physically based model for crack formation. *Geoderma*, 125(3-4):213–223.

[13] Musielak, G. and Śliwa, T. (2012). Fracturing of clay during drying: Modelling and numerical simulation. *Transport in porous media*, 95:465–481.

[14] Peron, H., Delenne, J., Laloui, L., and El Youssoufi, M. (2008). Discrete element modeling of drying shrinkage and cracking of soils. *Computers and Geotechnics*, 36:61–69.

[15] Hori, M., Oguni, K., and Sakaguchi, H. (2005). Proposal of FEM implemented with particle discretization for analysis of failure phenomenon. *Journal of the Mechanics and Physics of Solids*, 53:681–703.

[16] Oguni, K., Wijerathne, M. L. L., Okinaka, T., and Hori, M. (2009). Crack propagation analysis using PDS-FEM and comparison with fracture experiment. *Mechanics of materials*, 41(11):1242–1252.